Journal of Sound and Vibration (1998) **215**(5), 1043–1064
Article No. sv981619

REMOTE IDENTIFICATION OF IMPACT FORCES ON LOOSELY SUPPORTED TUBES: PART 2—COMPLEX VIBRO-IMPACT MOTIONS

J. Antunes and M. Paulino*
Instituto Tecnológico e Nuclear, *Applied Dynamics Laboratory*, *ITN/ADL*, 2686 *Sacavém Codex*, *Portugal*

AND

P. Piteau
Commissariat à l'Energie Atomique, *Département de Mécanique et Technologie CEA/DMT*, 91191 *Gif-sur-Yvette Cedex*, *France*

(*Received* 21 *April* 1997, *and in final form* 10 *March* 1998)

In a previous paper, techniques were presented, based on response measurements at remote locations, for the experimental identification of the flexural wave-guide propagation parameters and for recovering the impact forces. Numerical simulations and experiments were presented, for simple *isolated impacts*. Those basic results showed that such an inverse problem can be successfully attempted, and a good agreement was found between direct measurements and the remotely identified impact forces. However, when subject to flow-induced vibrations, the loosely supported tubes display very *complex rattling* motions—with the impact-generated primary waves completely immersed in countless wave reflections travelling between the tube boundaries. As a consequence, the multiple-impact patterns of tube-support interaction are much more difficult to identify than isolated force spikes. In this paper, the authors move a step further towards the identification of impacts for realistic tube vibrations. To deal with complex vibro-impact regimes, a signal-processing technique is presented for separating the multiple wave sources, which uses the information provided by a limited number of vibratory transducers. This technique can be applied to both non-dispersive and dispersive waves and is therefore useful for all kinds of beam motions. Such a method is instrumental in separating the primary impact-generated flexural waves from severe background contamination. This enables the straightforward identification of complex rattling forces at a loose support. Extensive results are given in order to assert the numerical conditioning of the technique used to identify the impact forces, the optimal location of the transducers used in the identification procedure, and the sensitivity of the identification method to noise contamination. Overall, results are quite satisfactory, as the complex identified impact forces compare favourably with direct measurements.

1. INTRODUCTION

Flow-induced vibrations of heat-exchanger tube bundles and nuclear fuel rods are important issues concerning component life and plant availability. Excitation by the flow turbulence and possible fluid-elastic phenomena may lead to a premature failure of the component due to material fatigue or to vibro-impact wear of the gap-supported tubes. Predictive methods have been developed to analyze the tube vibratory responses and wear

* Visiting MSc. Student from Faculdade de Ciências e Tecnologia/Universidade Nova de Lisboa (FCT/UNL), Portugal.

0022–460X/98/351043 + 22 $30.00/0

for realistic multi-supported bundles and flow configurations [1–17]. Validation of these predictive techniques, which is currently being pursued by the authors and others, has been achieved through laboratory experiments [18–28].

Laboratory work on vibro-impacting tubes involves carefully instrumented test tubes and tube-supports—see, for instance reference [24]. Such experimental conditions are seldom possible for real field components, due to space limitations and to the severe environment conditions (temperature, radiation) which prevent an adequate instrumentation of the tube supports. Therefore, the tube–support impact forces cannot be easily monitored under real operating conditions. Identification techniques that enable the diagnosis of tube–support interaction, based on remote vibratory measurements, will be quite valuable—for validating the predictive methods, as well as for condition-monitoring of the real components. These issues are being addressed by the authors in a series of papers.

Previous work in this field include papers by Whiston [29] and Jordan and Whiston [30], who discussed theoretical and experimental aspects related to the remote identification of impact forces. These authors modelled the flexural propagation waves in the frequency domain using a Timoshenko beam model without damping. In his book and in a series of related papers, Doyle [31] followed a similar approach. These authors also presented satisfactory experimental results provided by single impacts acting on long beams, in such a way that wave reflections at the boundaries do not interfere seriously with the direct wave used for identification proposes. Lin and Bapat [32, 33] presented methods for estimation of the impact forces and the support gap in a single-degree-of-freedom system, respectively, for sinusoidal and random excitations. The extension of these methods to a beam with a single non-linear gap-support was proposed by using a modal approach in the frequency domain [34]. Busby and Trujillo [35] presented a similar approach, in which the force identification is achieved in the time domain. The extension of these methods to multi-supported beams—which display an ill-defined (or even unknown) modal basis—seems problematic. In a recent paper, Wu and Yeh [36] discussed the problem of source separation, for several simultaneous impacts, using a time-domain approach. The so-called cepstral methods of deconvolution, which may be quite useful when dealing with non-dispersive phenomena, have been used very seldom for dispersive flexural waves [37].

In Part 1 de Araújo *et al*. [38] presented techniques, based on response measurements at remote locations, for the experimental identification of the flexural wave-guide propagation parameters and for recovering an impact force and impact location. Experimental results showed that these inverse problems can be successfully addressed and a good agreement was found between direct measurements and the remotely identified impact forces. However, as in most other work published until now, our numerical simulations and experiments were presented for simple *isolated impacts*. Figures 12(a) and (b) of Part 1 show the experimental wave generated by a single impact on a beam of finite length at two locations. One can notice the arrival of the direct wave followed by the reflections from the boundaries. A wave dispersion effect is clear, as is the increasing significance of wave reflections when the motion transducer is far from the impact location. Also shown is the simple approach used to suppress wave reflections—the experimental wave was truncated just before the arrival of the first reflection and replaced by an ''analytic continuation'', based on the theoretical wave solution of an infinite beam excited by a force pulse. From such ''cleaned'' direct waves, the excitation force shown in Figure 14 (Part 1) was identified by using the theoretical formulation presented in our previous paper.

However interesting, such experiments are still remote from the operating conditions of real-life components. Indeed, when subject to flow-induced vibrations, loosely supported tubes display very *complex rattling* motions. The primary waves generated by isolated

impacts enable clean force identifications to be made, because they are usually well separated from the secondary waves generated at the tube boundaries (a signal lasting only 0·01 s is adequate for the identification of an isolated impact). However, such is not the case for complex rattling regimes, when the impact-generated primary waves are completely immersed in countless wave reflections travelling between the tube boundaries (for vibro-impact motions, identification should be based on signals lasting 1 s or more). Under such conditions, the simple "cleaning" approach previously described is obviously not adequate. Furthermore, the secondary waves cannot be processed by using common reflection functions, as typically done for very basic systems, because the boundary conditions are usually unknown or ill-defined in multi-supported tubes. As a consequence, the multiple-impact patterns of real tube–support interaction are much more difficult to identify than isolated force spikes.

The main difficulty with inverse problems is ill-conditioning—physical or numerical—of the transformation/propagation operators which describe the phenomena. This leads to inverse formulations which are very sensitive to noise contamination of the measured signals. Problems may be partially overcome by regularization of the transformation operators, by using several methods, namely, singular value decomposition, incorporation of physical constraints and optimization techniques [38–41]. In the context of vibro-impact system identification, ill-conditioning difficulties are enhanced due to the dispersive nature of flexural waves. Techniques to deal with inverse problems in other fields have been presented by Jeffrey and Rosner [42], Dimri [43] and Parker [44].

In the first part of this paper, the main theoretical equations for the propagation of flexural waves are recalled, for completeness. Then, a signal processing technique is presented which makes possible the separation of multiple wave sources, and which uses the information provided by a limited number of vibratory transducers. This technique can be applied to both non-dispersive and dispersive waves and is therefore useful for all kinds of beam motions. Such a method is instrumental in separating the primary impact-generated flexural waves from the severe background contamination by secondary wave reflections. This enables the straightforward identification of complex rattling forces at a loose support. The paper presents extensive results in order to assert the numerical conditioning of the technique used to identify the impact forces, the optimal location of the transducers used in the identification procedure, and the sensitivity of the identification method to noise contamination. Experiments were performed with a long steel beam (approximate length 6 m) with non-anechoic boundaries. Excitation was provided by a pair of small inertial shakers driven by banded white noise, in order to simulate the flow turbulence. Impacts were generated at an instrumented support presenting a gap. Vibratory measurements and impact force identifications were based on the responses provided by accelerometers located far from the gap-support. Overall, results were quite satisfactory, as the identified rattling forces compare favourably with the direct measurements.

2. THEORETICAL FORMULATION

As shown by de Araújo *et al*. [38], simple Bernoulli–Euler theory for flexural vibrations proved to be adequate for identification of the tube–support impacts. Upon assuming a viscous damping model, the small-amplitude flexural response of a beam (with constant cross-section) is described by [45, 46]

$$EI\,\partial^4 y/\partial x^4 + \rho A\,\partial^2 y/\partial t^2 - N\,\partial^2 y/\partial x^2 + \eta\,\partial y/\partial t = F(t), \tag{1}$$

where $F(t)$ is the external force and $y(t)$ is the dynamic vibratory response, E is the Young's modulus and ρ is the mass density of the beam, A is the area and I is the moment of inertia of the cross-section, N is the axial tension on the beam and η is a viscosity coefficient. Here, parameters E, ρ, A, I, N and η are assumed constant along the beam. (A list of nomenclature is given in the Appendix). Upon neglecting the axial tension and damping effects, a solution for equation (1) may be obtained in the form

$$y(x, t) = \sum_n (C_{1n}\, \mathrm{e}^{-\mathrm{i}k_n x} + C_{2n}\, \mathrm{e}^{\mathrm{i}k_n x} + C_{3n}\, \mathrm{e}^{-k_n x} + C_{4n}\, \mathrm{e}^{k_n x})\, \mathrm{e}^{\mathrm{i}\omega_n t}, \tag{2}$$

where, for each circular frequency ω_n, the parameter k_n is given by the so-called dispersion relation:

$$k_n = [\rho A/EI]^{1/4}\sqrt{\omega_n} \equiv \mathscr{C}\sqrt{\omega_n}, \tag{3}$$

and the parameters C_{1n} to C_{4n} are frequency dependent. The first and second terms of solution (2) are propagating waves, while the third and fourth terms are non-propagating (evanescent). As discussed in Part 1, the non-propagating terms can be disregarded—as far as the remote identification problem is concerned—provided all motion transducers are located far from singularities such as the tube boundaries and excitation locations.

Upon assuming that the beam response $y_0(t) \equiv y(0, t)$ is measured at location $x = 0$ during time T, the coefficients Y_n of the spectral form

$$y_0(t) = \sum_n Y_n\, \mathrm{e}^{\mathrm{i}\omega_n t} \tag{4}$$

may be computed from Fourier analysis. Then, the propagated forward and backward travelling waves can be predicted at any other location x by using

$$y_f(x, t) \cong \sum_n Y_n\, \mathrm{e}^{-\mathrm{i}k_n x + \mathrm{i}\omega_n t}, \qquad y_b(x, t) \cong \sum_n Y_n\, \mathrm{e}^{\mathrm{i}k_n x + \mathrm{i}\omega_n t}. \tag{5}$$

On the other hand, upon assuming that a force $F(t)$ is applied at location $x = 0$ during a time T, and using the spectral form

$$F_y(t) = \sum_n F_n\, \mathrm{e}^{\mathrm{i}\omega_n t}, \tag{6}$$

then the beam response at location x is given by [47]

$$y_f(x, t) \cong \frac{1}{4EI} \sum_n \frac{F_n}{k_n^3}\, \mathrm{i}\, \mathrm{e}^{-\mathrm{i}k_n x + \mathrm{i}\omega_n t}, \qquad y_b(x, t) \cong \frac{1}{4EI} \sum_n \frac{F_n}{k_n^3}\, \mathrm{i}\, \mathrm{e}^{\mathrm{i}k_n x + \mathrm{i}\omega_n t}. \tag{7}$$

These equations will be used to convert from the impact forces to response measurements and for force estimation. Equations to alternative equations (5) and (7) may be obtained when dealing with velocity, acceleration and strain signals. If the axial tension N and damping effects are included, the dispersion relation is more complex than given in equation (3), and k_n will display both real and imaginary parts. de Araújo *et al*. [38] presented such results in detail. As noted in Part 1, damping effects are often quite low and can be safely neglected. The preceding theoretical formulation is adequate because, in this work, we are concerned with beams which present a single gap-support. Limitations on the spatial distribution of impact boundary conditions and the frequency range of propagating waves have been thoroughly discussed by Babitsky and Krupenin [48] and Krupenin and Veprik [49], when analyzing systems with a large number of limiters.

In practice, manipulation of the preceding formulations can be conveniently achieved by fast Fourier transforming all the time-domain signals. Then propagation phenomena in the frequency domain are given by simple products of functions. Finally, the time-domain estimated results are obtained by inverse Fourier transforms. The same routine applies when computing the inverse problems. As noted in Part 1, due to the finite length of discrete Fourier transforms, signals usually display wraparound artefacts after the frequency-domain processing. Such spurious effects are usually prevented by windowing the time-data. Because this technique also leads to significant distortions of the signals—which should be avoided for identification purposes—the authors chose to process 10% more data than displayed. This simple approach was found effective in disguising wraparound effects.

Signal filtering is also an important aspect of the identification procedure. In section 6 the need for low-pass or high-pass filtering of the data is discussed, as well as the criteria for choosing the filtering frequencies. In this paper, data blocks were batch-processed in the frequency domain. Hence, filtering was simply achieved by zeroing the Fourier coefficients of the transformed signals in the frequency ranges to be filtered-out. Because this practical filtering technique is non-causal, moderate signal distortions may be noticed in the identified impact forces. More sophisticated signal-denoising techniques—for instance using wavelets [50], which are particularly well suited for non-stationary signals—can obviously be used.

3. IDENTIFICATION OF IMPACT FORCES

In order to illustrate the main difficulty in the identification problem, Figure 1 shows numerical simulations of the propagation waves generated by a typical impact (a) on an infinite beam (b) and on a beam with finite length (c). These simulations were produced by using the method presented in section 2, upon assuming the following physical parameters: $E = 2 \times 10^{11}$ Pascal, $\rho = 7{\cdot}4 \times 10^3\,\mathrm{kg/m^3}$, $A = 2{\cdot}95 \times 10^{-4}\,\mathrm{m^2}$, $I = 8{\cdot}56 \times 10^{-10}\,\mathrm{m^4}$ and $N = \eta = 0$. Here the multiple reflections in the finite beam (with length 5·805 m) were generated by assuming pinned–pinned boundaries with 5% dissipation at every reflection. If no noise is injected into the system, equation (7) enables a precise inversion of the wave response (b) to be made, so that the force time-history (a) can be exactly recovered. However, such is not the case for the finite-length beam, and the straight inversion of the wave response (c) would lead to the completely erroneous impact force (d). Therefore, it is essential to isolate the primary waves from the background secondary reflections, in order to overcome this problem.

For very simple systems, the wave separation may be attempted if the boundary conditions are perfectly known, because wave reflections can then be precisely formulated [31, 46]. However, this is seldom possible in real-life components and certainly not the case for multi-supported tube bundles. The authors' approach is to perform the wave separation using a limited number of vibratory transducers at two remote locations. These encompass a section of the beam which contains the gap-support (located at x_0)—see Figure 2(a). The right-travelling and left-travelling waves can then be separated by using the simple frequency-domain formulation to be presented next.

Consider the pair of transducers located on the left side of the beam within a close distance ℓ—see Figure 2(b). Each transducer j senses a signal $z_j(t)$ which is the sum of the right-travelling wave $y_{aj}(t)$ plus the left-travelling wave $y_{bj}(t)$. Hence

$$z_1(t) = y_{a1}(t) + y_{b1}(t), \qquad z_2(t) = y_{a2}(t) + y_{b2}(t). \tag{8, 9}$$

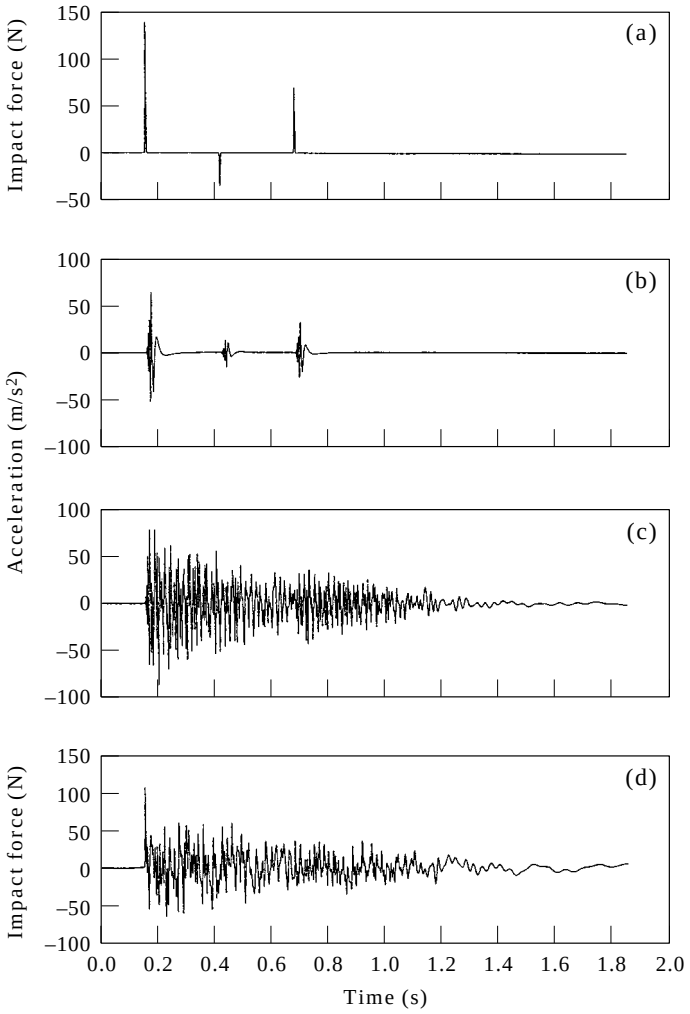

Figure 1. Numerical simulation of an impact and the flexural waves generated on a beam: (a) impact force; (b) response wave on a beam with infinite length; (c) response wave on a finite-length beam; (d) direct force identification from the wave response of the finite-length beam (b) and (c). Measurement in location $x_4 = 5{\cdot}002$ m.

By Fourier-transforming equations (8) and (9), equation (9) can be easily written in terms of the waves sensed by the first transducer:

$$Z_1(\omega) = Y_{a1}(\omega) + Y_{b1}(\omega), \qquad Z_2(\omega) = Y_{a1}(\omega)\, \mathrm{e}^{-\mathrm{i}k(\omega)(x_2 - x_1)} + Y_{b1}(\omega)\, \mathrm{e}^{\mathrm{i}k(\omega)(x_2 - x_1)}, \tag{10, 11}$$

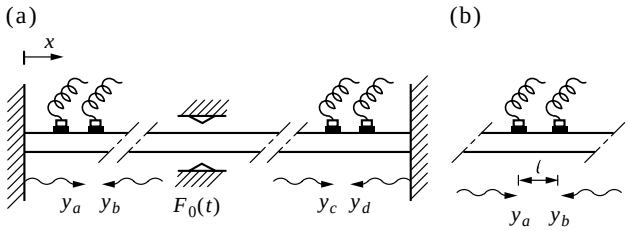

Figure 2. (a) Typical set-up for the wave separation and impact-force identification; (b) detail of a pair of close trasducers.

or, in matrix form, with $\ell = x_2 - x_1$,

$$\begin{Bmatrix} Z_1(\omega) \\ Z_2(\omega) \end{Bmatrix} = \begin{bmatrix} 1 & 1 \\ e^{-ik(\omega)\ell} & e^{ik(\omega)\ell} \end{bmatrix} \begin{Bmatrix} Y_{a1}(\omega) \\ Y_{b1}(\omega) \end{Bmatrix}, \tag{12}$$

and the Fourier transform of the separated waves is obtained by inversion of equation (12) as

$$\begin{Bmatrix} Y_{a1}(\omega) \\ Y_{b1}(\omega) \end{Bmatrix} = [\mathscr{M}_{12}(\omega)]^{-1} \begin{Bmatrix} Z_1(\omega) \\ Z_2(\omega) \end{Bmatrix}. \tag{13}$$

In a similar way, the pair of transducers located on the right side of the beam is used to obtain

$$\begin{Bmatrix} Y_{c4}(\omega) \\ Y_{d4}(\omega) \end{Bmatrix} = [\mathscr{M}_{34}(\omega)]^{-1} \begin{Bmatrix} Z_3(\omega) \\ Z_4(\omega) \end{Bmatrix}. \tag{14}$$

The time-domain separated waves are easily obtained by inverse Fourier-transforming the arrays $Y_{a1}(\omega)$, $Y_{b1}(\omega)$, $Y_{c4}(\omega)$ and $Y_{d4}(\omega)$. One may notice that this kind of transducer pairing has also been used for a completely different purpose—the measurement of sound or vibration intensity [51–53]. However, the aim in such applications is not to recover the time-histories of separated waves but to obtain a vector-mapping of the energy-flow in the system.

From equations (13) and (14), two estimates of the impact force can be obtained in the following manner:

$$F_0^{(1)}(t) = \mathscr{F}^{-1}\left[\frac{Y_{b1}(\omega) - Y_{d4}(\omega)G_{41}(\omega)}{\tilde{G}_{01}(\omega)}\right], \qquad F_0^{(2)}(t) = \mathscr{F}^{-1}\left[\frac{Y_{c4}(\omega) - Y_{a1}(\omega)G_{14}(\omega)}{\tilde{G}_{04}(\omega)}\right]. \tag{15, 16}$$

Here the propagation functions $G_{ij}(\omega)$ and $\tilde{G}_{0j}(\omega)$ are given as

$$G_{ij}(\omega) = e^{-ik(\omega)(x_i - x_j)}, \qquad \tilde{G}_{0j}(\omega) = (i/4EIk(\omega)^3)\, e^{-ik(\omega)(x_0 - x_j)}, \tag{17}$$

Notice that, in equation (15), the left-travelling reflection measured at location 4 must be propagated and subtracted from the left-travelling wave measured at location 1, prior to the force identification. A similar action is taken concerning the right-travelling waves used in equation (16). Formulation (17) was established by assuming that the waves are sensed by displacement transducers. For other types of transducers, simple modifications apply—for example, a factor $-\omega^2$ is introduced in formulation $\tilde{G}_{0j}(\omega)$ when accelerometers are used.

Figure 3 shows the impact force identified at location $x_0 = 2{\cdot}236$ m from the numerically simulated response illustrated in Figure 1(c)—the finite-length beam. For the identification procedure, the wave responses at locations $x_1 = 0{\cdot}805$, $x_2 = 0{\cdot}855$, $x_3 = 4{\cdot}953$ and $x_4 = 5{\cdot}003$ m were used. Four levels of "measurement" noise were assumed (0, 10, 20 and 50%), when using random signals of adequate levels to pollute the clean responses. One can notice that the identification method is robust to noise contamination effects. The small

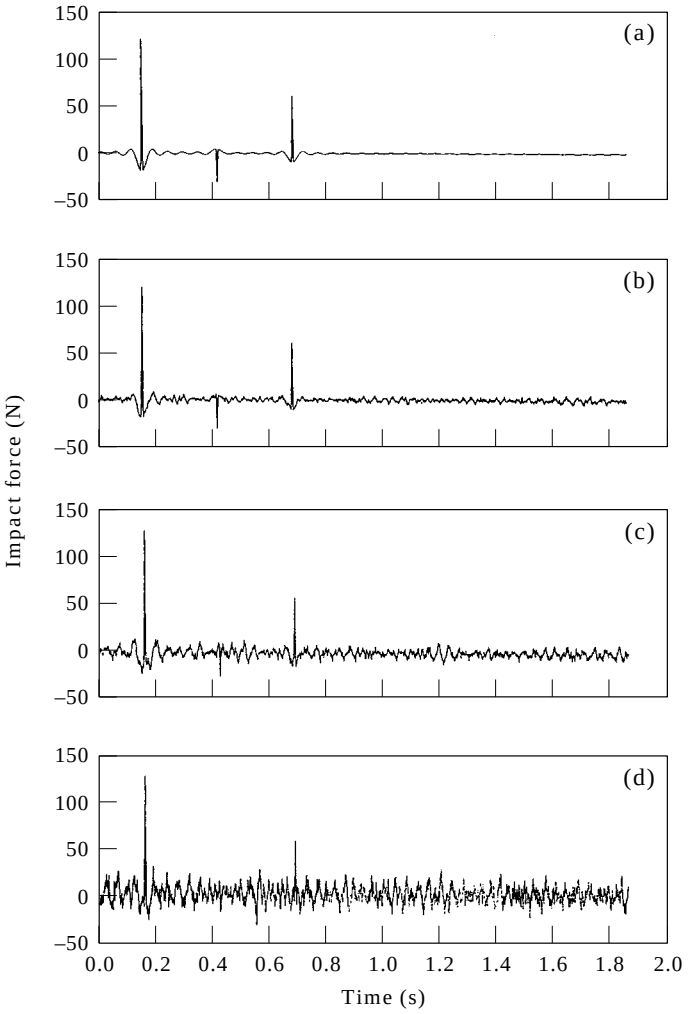

Figure 3. Impact force identifications using numerical simulations of a finite-length beam: (a) identification from clean vibratory responses; (b) with noise contamination 10%; (c) with noise contamination 20%; (d) with noise contamination 50%.

distortion of the identified force is due to the high-pass filtering (at 20 Hz) which was applied to the signals prior to identification—this aspect will be discussed in section 6.

Here, the same dispersion relation was used for generating the wave responses and also in the identification procedure. However, simulations also showed that the quality of the identified results is quite sensitive to the phase velocity assumed in the identification. Therefore, it is very important that such a parameter is carefully adjusted when processing experimental results, as it must follow closely the true value. Dispersion relations such as equation (3) are very useful to obtain a first estimate of the wave propagation parameters. The initial estimate must then be refined, by using an optimization procedure to minimize the identification error—see reference [38] for details. It will be shown in the next section that, when the dispersion relation is properly modelled, experimental identifications are feasible and robust enough.

4. EXPERIMENTAL SET-UP

Figure 4(a) shows the test system, consisting of a stainless steel AISI 304 laminated beam with cross-section $50 \times 5{\cdot}9$ mm and length about 6 m. The beam is supported only at the extremities, with the larger surfaces in the vertical position, by using (almost) clamped–clamped boundary conditions. The beam supports are mounted on heavy concrete blocks. The Young's modulus of the beam is about 2×10^{11} Pascal and the mass density is about $7{\cdot}9 \times 10^3$ kg/m^3. Errors of $\pm 1\%$ were found in the cross-section dimensions along the beam and an incertitude of $\pm 5\%$ is expected in the values of E and ρ. Thus, the propagation parameter $\mathscr{C} = [\rho A/EI]^{1/4}$ (see equation (3)) is estimated to lie

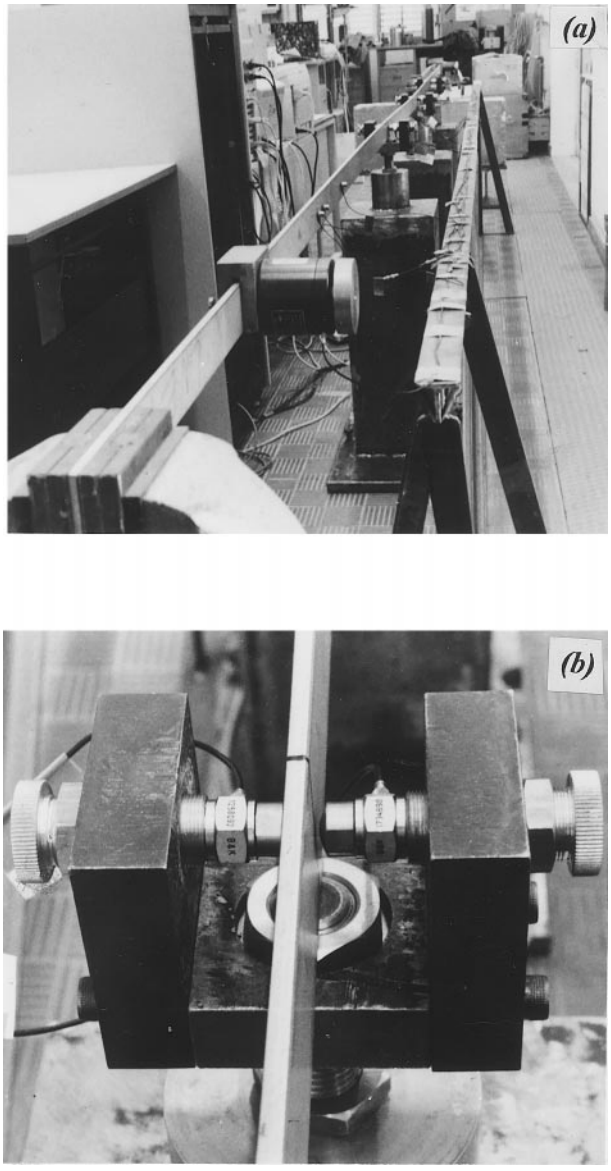

Figure 4. (a) General view of the experimental set-up; (b) detail of the instrumented support.

between 0·332 and 0·352. Dissipative effects are very low (modal damping was less than 0·1%, for the first beam mode).

Figure 4(a) also shows the miniature accelerometers Brüel and Kjaer (B&K) 4375 used to measure the vibratory responses. These were located according to several configurations, as discussed later. Up to six accelerometers were used to sense the "useful" horizontal waves (direction y), while another accelerometer monitored the residual vibrations in the vertical direction. Almost planar motions of the beam were observed, with residual levels in the orthogonal direction always within 10% of the main motion amplitudes. The accelerometers used in these experiments were purposefully selected and mounted without aiming at better-than-average precision or phase matching specifications. Indeed, from preliminary calibrations, the magnitude errors are expected within 10% and phase errors should lay within $\pm 5^{\circ}$. These results apply to the mounted transducers, in the frequency range below 4 kHz.

Figure 4(b) shows the instrumented support, consisting of a rigid fixture mounted on a heavy column, in order to minimize the residual vibrations. Impacts were always imposed along the horizontal direction. Two calibrated threaded stops enabled us to adjust precisely the support gaps. Each stop was provided with a piezoelectric force transducer B&K 8200, equipped with a metallic tip. The experiments reported pertain to a support gap adjusted at $+0{\cdot}5/-0{\cdot}5$ mm. Excitation of the beam was provided by two inertial shakers located near the beam boundaries, as shown in Figure 4(a). The shakers were driven by two uncorrelated white-noise signals—filtered outside the range $2 \sim 2000$ Hz—in order to simulate approximately the random excitation by the flow turbulence. The excitation level (set at about 10 N_{rms}) was enough to induce realistic vibro-impact motions. It is important to stress that the identification algorithm had to cope, in addition to the impact generated wave reflections, with the primary and reflected random waves generated by the shakers.

Data acquisition was performed by using a National Instruments (AT-MIO-16F5) 8-channel 12-bit card, having a digitizing frequency of 20 kHz and signal blocks of $1 \sim 1{\cdot}5$ s. This is consistent with the frequency range where signals displayed significant energy (up to $4 \sim 5$ kHz). For the reasons presented in Part 1, no anti-aliasing filters were used in the present experiments. Data processing and system identification were performed by using PC-based software, which was developed within a MATLAB computing environment.

5. IDENTIFICATION RESULTS

To provide a feel for the actual performance of the identification approach, some experimental results are now presented, obtained by using the minimum number of response transducers (e.g., four accelerometers). These were located as noted in section 4, whereas the instrumented support was located at $x_0 = 2{\cdot}401$ m. In section 6, the optimal number and location of the response transducers in connection with the conditioning of the identification procedure will be discussed thoroughly. As will be demonstrated, the chosen distance of 50 mm between closer transducers is nearly optimal.

Figure 5(a) shows a sample of the impact force, as measured at the instrumented support. The corresponding response of the first accelerometer is illustrated in Figure 5(b). A comparison with the experimental signals of Part 1 stresses the difficulty of the new identification problem. Indeed, Figure 5(c) shows how bad results can be if one attempts to recover the impact force by a direct inversion as in equation (7). Figure 6 presents two estimations of $F_0(t)$ obtained by using the identification method presented in section 3.

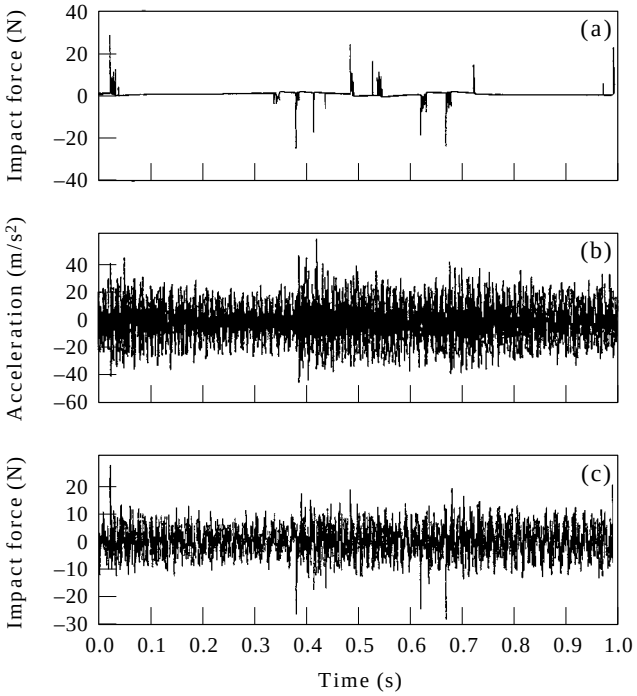

Figure 5. (a) Measured impact force time-history; (b) sample of a response time-history; (c) force identification using naive direct inversion.

These results were produced by using the dispersion relation (3), after an optimal value of the propagation parameter $\mathscr{C}$ was identified (see Part 1).

The much improved estimations of Figure 6 can be further refined by using the fact that they correlate very well when impact forces arise and very badly when there is only

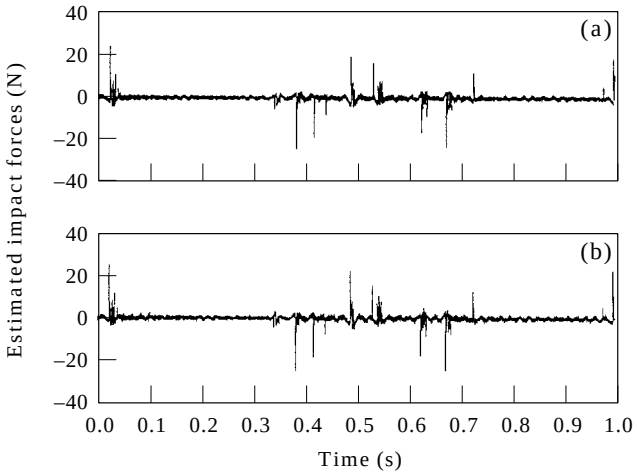

Figure 6. Two identifications of the impact force based on the present approach (see section 3): (a) estimated "impact forces" (from right-travelling waves); (b) estimated "impact forces" (from left-travelling waves).

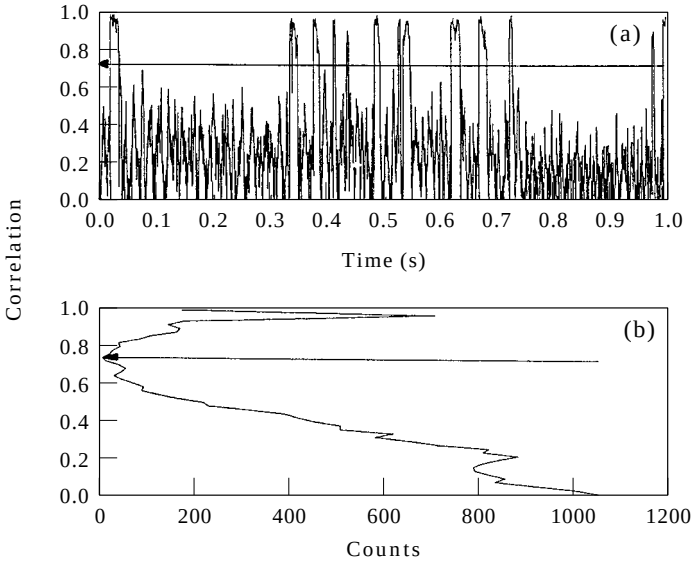

Figure 7. Moving cross-correlation $\mathscr{R}(t)$ between force estimates; (b) optimal decision level based on the minimum of the histogram of $\mathscr{R}(t)$.

background noise. Therefore, these estimations were processed using a "moving cross-correlation" defined as

$$\mathscr{R}(t) = \frac{\displaystyle\int_{t-\Delta T}^{t+\Delta T} (F_0^{(1)}(t) - \bar{F}_0^{(1)})(F_0^{(2)}(t) - \bar{F}_0^{(2)})\,\mathrm{d}t}{\left[\displaystyle\int_{t-\Delta T}^{t+\Delta T} (F_0^{(1)}(t) - \bar{F}_0^{(1)})^2\,\mathrm{d}t \int_{t-\Delta T}^{t+\Delta T} (F_0^{(2)}(t) - \bar{F}_0^{(2)})^2\,\mathrm{d}t\right]^{1/2}}, \tag{18}$$

where the size of the moving window ($2\Delta T$) is based on the time-scale of individual impacts (a value of 5×10^{-3} s was used for this system). Then, a better estimation of the impact force is computed by taking the average of both force estimates when $\mathscr{R}(t)$ is higher than a suitable value (e.g., when impacts arise), and assuming a null amplitude when $\mathscr{R}(t)$ is lower (e.g., no impacts).

Figure 7(a) displays the result of equation (18), for the signals presented in Figure 6. One may notice that the correlation increases significantly when impacts arise. Under blind conditions, the choice of a suitable level of $\mathscr{R}$ for discriminating impacts from the background noise is obviously open to discussion. However, based on the known true force, it was found that a good criteria is given by the level of $\mathscr{R}$ corresponding to a minimum in the histogram of the moving-correlation function—see Figure 7(b). In retrospect this is logical, because $\mathscr{R}(t)$ is low for a long time due to noise effects, when there are no impacts. However, $\mathscr{R}(t)$ also displays high values for a significant time during the multiple impacts (rattling). Therefore, the least time (e.g., the histogram minimum) is consumed during the beam-support approach and release. The procedure suggested has the obvious advantages that it can be completely automated and is free from subjective decisions.

A comparison between the measured force and the refined identification is presented in Figure 8(a). A detail of the force time-histories is also given in Figure 8(b). Correlation

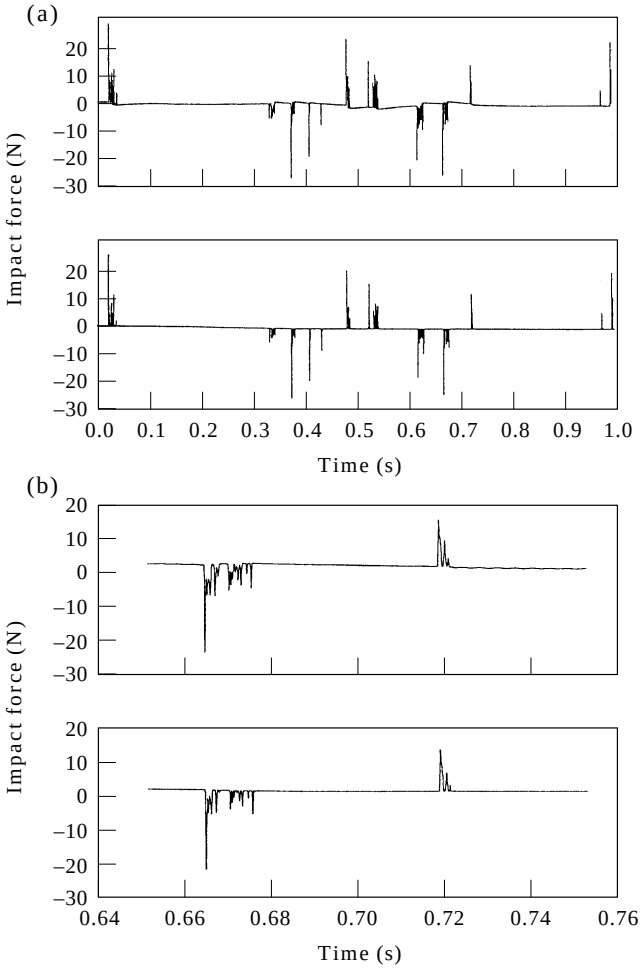

Figure 8. (a) Measured and final identified impact forces; (b) detail of the force time-histories. Measured force (top); ''optimal'' force identification, filtering at 50–5000 Hz (bottom).

coefficients between the measured force and the results from the identification methods are shown in Table 1. The final results are obviously very encouraging.

6. IMPORTANT IDENTIFICATION ASPECTS

After the previous framework, more subtle aspects related to the identification problem are now discussed, namely, numerical conditioning of the identification technique, optimal

TABLE 1
Correlation coefficients between the measured and estimated impact forces

Identification method	Correlation coefficient
Direct naïve inversion	0·19
Using wave separation	0·79
After final ''cleaning''	0·90

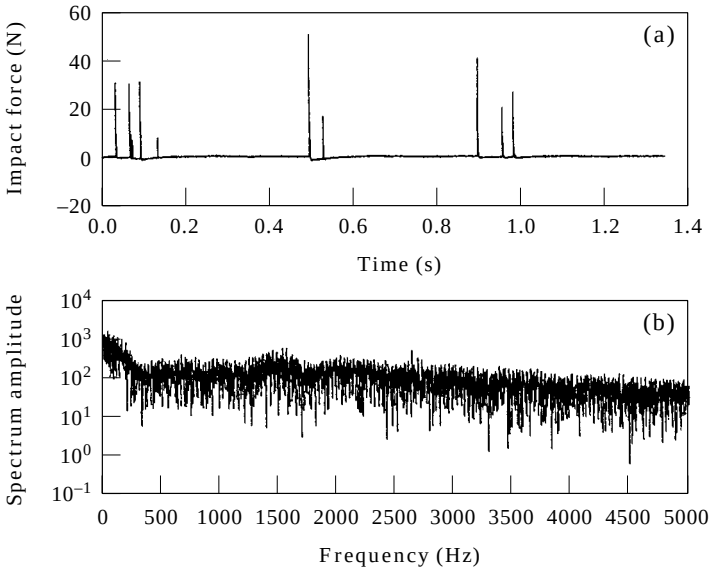

Figure 9. (a) Measured impact force time-history; (b) measured impact force spectrum.

number and location of the vibratory transducers; and signal filtering. All the identification results presented here do not include the final "cleaning" procedure described in section 5, in order to emphasize the points discussed.

Figures 9(a) and (b) show an experimentally measured impact force (in this case single-sided) and the corresponding spectrum, which is quite smooth. Figure 10(a) presents the unfiltered identified result using four accelerometers. The distance between closer transducers, 300 mm, is now greater than in the preceding identifications. It is clear that the identified force is useless, due to spurious high-amplitude contamination. As shown in Figure 10(b), the spectrum of the identification result presents high-amplitude peaks at well-defined frequencies. This effect is clearly explained by Figure 10(c), which shows the *condition number Cn* of the wave-separation operators $[\mathscr{M}_{12}(\omega)]$ or $[\mathscr{M}_{34}(\omega)]$—see equations (13) and (14)—as a function of frequency. Here Cn is defined as the ratio of the lowest and highest singular-values of the wave-separation matrixes:

$$Cn = \sigma_{min}/\sigma_{max}. \tag{19}$$

Formulation (19), which is very convenient because $0 < Cn < 1$, is the inverse of a current definition of the condition number. When $Cn \to 0$, the matrix is almost singular and the inverse problem is very ill-conditioned. Conversely, $Cn \to 1$ means that inversion is well conditioned. If the inversion matrix is almost singular, any noise in the measurements will be unduly amplified, as shown at certain frequencies in Figures 10(b) and (c). The physical interpretation of the numerical ill-conditioning is that each pair of transducers is "blind" at all frequencies ω corresponding to wavelengths $\lambda(\omega)$ which are sub-multiples of the distance ℓ between the transducers. Figure 10(d) shows that low-pass signal filtering (at 400 Hz) may improve the identified results—however, at the expense of a highly distorted and severely clipped identification.

Figure 10 showed that higher distances between transducers lead to instability at several medium-to-high frequencies. Figures 11(a)–(c) show what happens when transducers are located closer (50 mm). Here there are much fewer frequencies leading to ill-conditioning, and spurious responses arise only at very low frequencies. Therefore, the high-pass filtered (at 50 Hz) identified force shown in Figure 11(d) is quite reliable.

The preceding examples stress the importance of choosing an optimal distance between transducers, in order to minimize spurious effects and signal filtering. This can be done by noticing that noise amplification arises whenever Cn is lower than about 0·2. Therefore, it is easy to compute the overall frequency range leading to ill-conditioning as a function of the distance ℓ_{12} between transducers. This is shown in Figure 12, for the propagation parameters of our experimental set-up, with a clear minimum at about 50 mm (the transducer distance used for the identification presented in section 5).

The preceding results suggest that identification may be improved if more than four transducers are used in order to eliminate ill-conditioning. Indeed, as demonstrated earlier by Gibiat and Laloë [54], two close transducers are well suited for higher frequency waves but give poor resolution in the lower frequency range. Conversely, two sufficiently distant

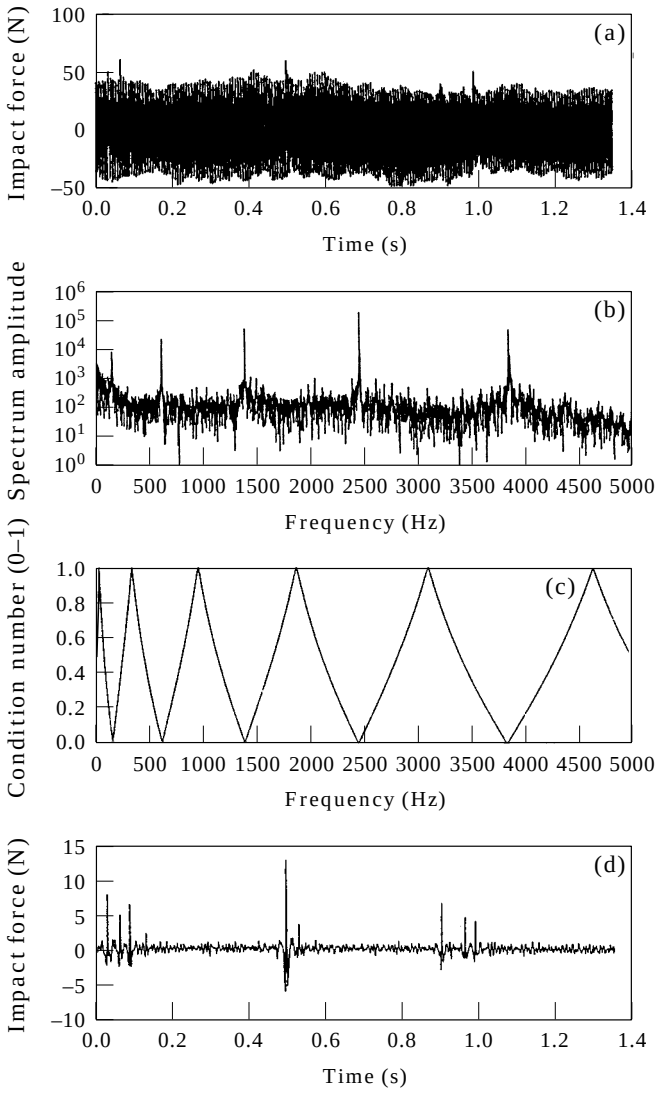

Figure 10. (a) Unfiltered impact force identification (four transducers, $\ell = 300$ mm); (b) unfiltered impact force identification spectrum; (c) condition number of the inversion operator; (d) low-pass filtered (at 400 Hz) impact force identification.

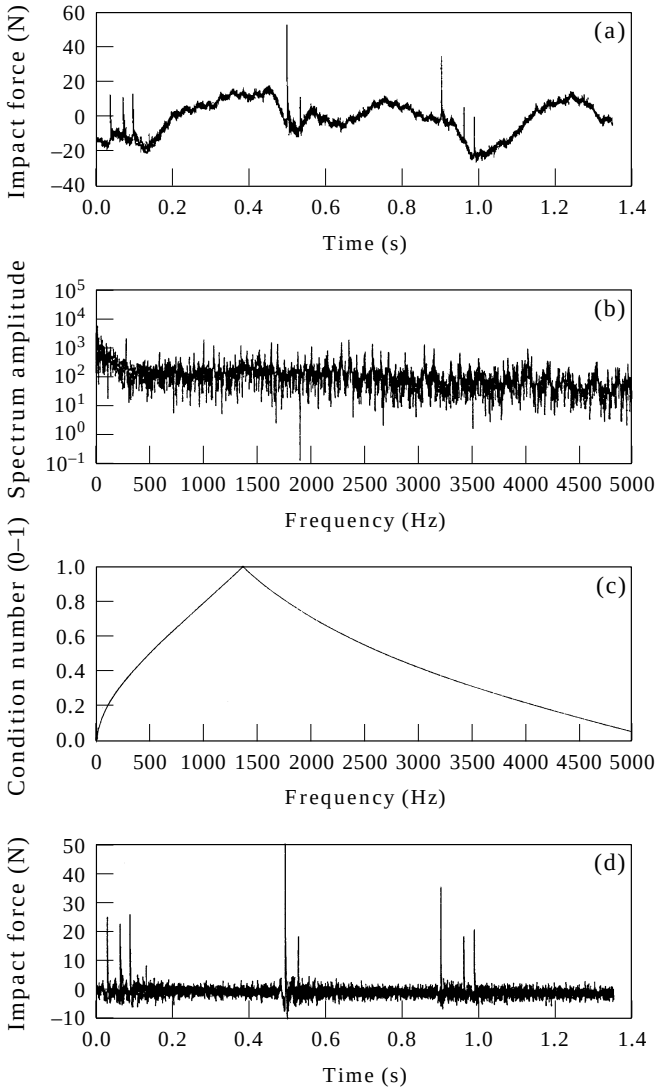

Figure 11. (a) Unfiltered impact force identification (four transducers, $\ell = 50$ mm); (b) unfiltered impact force identification spectrum; (c) condition number of the inversion operator; (d) high-pass filtered (at 50 Hz) impact force identification.

transducers are well suited for the lower frequency waves but rather inaccurate when processing higher frequencies. The optimal distance between transducers is about $\lambda/4$, for monochromatic waves. However, when dealing with wider-band waves, a given transducer configuration may be used optimally only in a limited frequency range. Following the above discussion, Gibiat and Laloë used—in their acoustical impedance measurements of woodwind music instruments—two microphone pairs: a close one when exciting (with acoustical chirps) their system in the low-frequency range and a more distant pair for higher frequencies.

This basic idea must be extended in order to deal with our impact-generated flexural travelling waves. Indeed, the frequency range of such waves is very wide, and frequency-band separation is obviously not a practical issue here. The authors' approach is to simultaneously use three transducers, two of them quite close and the third well

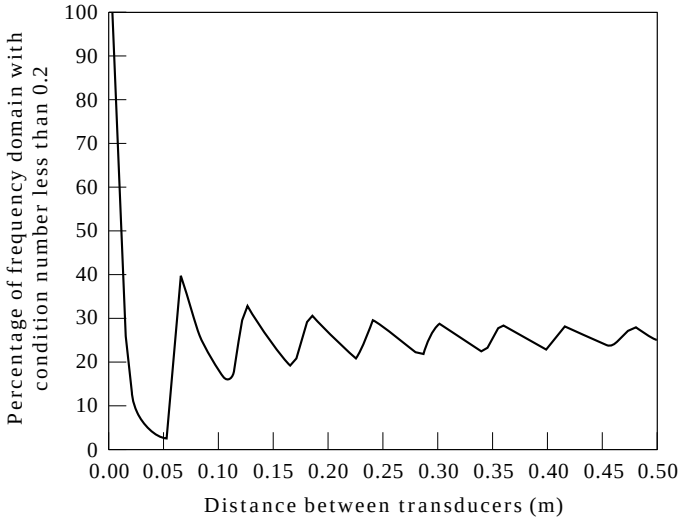

Figure 12. Frequency range leading to ill-conditioned identification as a function of the distance ℓ_{12} between transducers (four transducers).

separated. Hence, the mathematical inversion problem becomes better conditioned for a large range of frequencies, with improved results under noisy conditions. The wave-separation matrix is then oversized (three equations to separate two waves), so that a classic Moore–Penrose (minimum-norm) pseudo-inversion must be performed (see, for instance reference [40]),

$$[\mathscr{M}]^{+} = ([\mathscr{M}]^{*\mathrm{T}}[\mathscr{M}])^{-1}[\mathscr{M}]^{*\mathrm{T}}, \tag{20}$$

where $[\mathscr{M}]^{*\mathrm{T}}$ is the Hermitian transpose of the complex matrix $[\mathscr{M}]$. It can be proved that equation (20) leads to a minimization of the error, in the least-squares sense, between measured data and the fitted model.

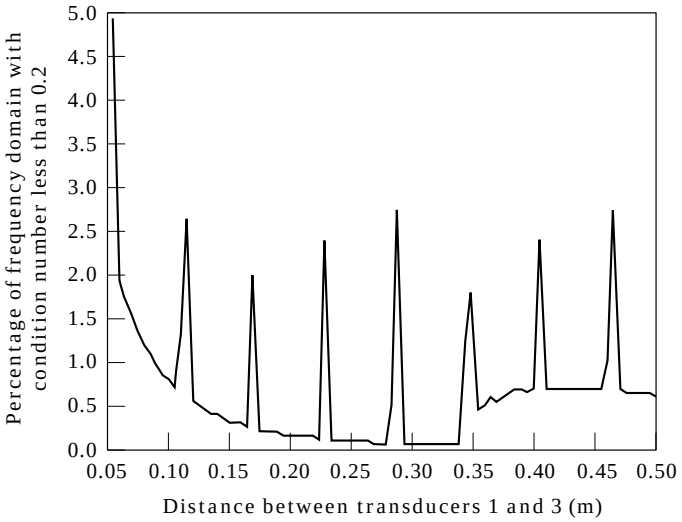

Figure 13. Frequency range leading to ill-conditioned identification as a function of the distance ℓ_{13} between transducers (six transducers, $\ell_{12} = 50$ mm).

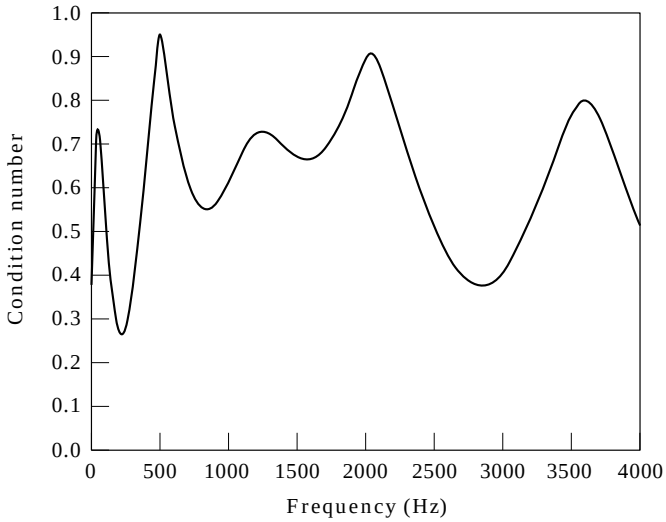

Figure 14. Condition number of the inverse operator (six transducers, $\ell_{12} = 50$ mm, $\ell_{13} = 270$ mm).

Consider now two sets of three transducers, with the closer ones at the previously computed optimum distance (50 mm). Figure 13 shows the overall frequency range leading to ill-conditioning, as a function of the distance ℓ_{13} between the farthest transducers. One can notice that there are several "bad" locations for the third transducer, and that optimal results should be obtained when $\ell_{13} \approx 270$ mm or $\ell_{13} = 300 \sim 340$ mm. Indeed, Figure 14 confirms that when using six transducers at distances $\ell_{12} = 50$ mm and $\ell_{13} = 270$ mm, the complete frequency range up to 4000 Hz is well conditioned.

The numerical simulations presented in Figure 15 support the preceding conclusions. One can notice that, under noisy conditions, the six-transducer identified force is a better

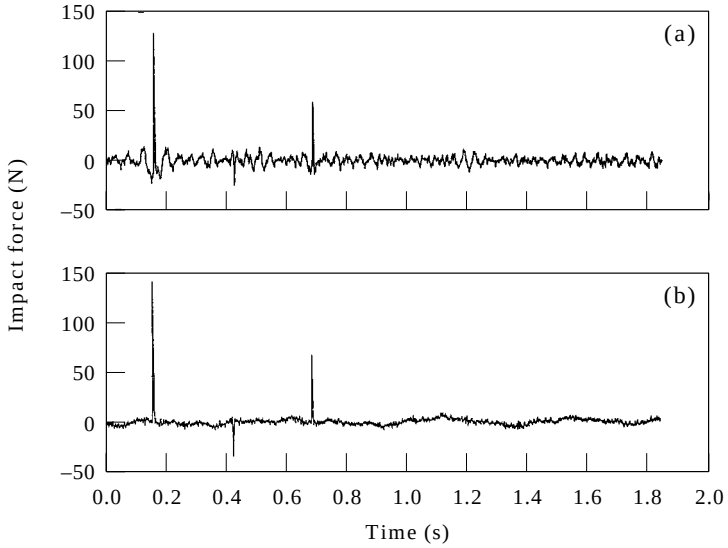

Figure 15. Identified impact force from a numerical simulation (20% noise contamination): (a) four tranducers, $\ell_{12} = 50$ mm, high-pass filter at 20 Hz; (b) six transducers, $\ell_{12} = 50$ mm, $\ell_{13} = 340$ mm, high-pass filter at 2 Hz.

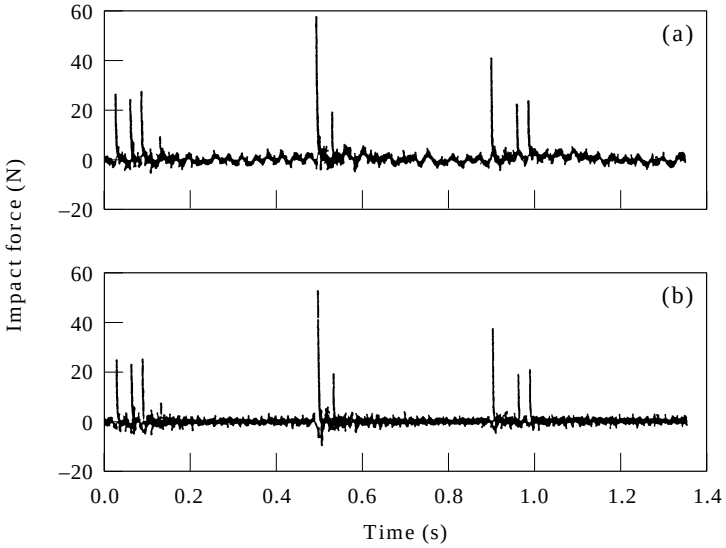

Figure 16. Experimental identification results (six transducers, $\ell_{12} = 50$ mm, $\ell_{13} = 340$ mm): (a) unfiltered impact force identification; (b) high-pass filtered (at 50 Hz) impact force identification.

approximation than the four-transducer identification. In particular, less filtering was needed to achieve good results.

The improvement of the experimental identifications when six transducers are used is less impressive. As expected, high-pass filtering is essential with the four-transducer set-up and almost useless when using six transducers—compare Figures 11(a) and 16(a). However, most of the impact energy lies in the medium-to-high frequency range, therefore moderate filtering of the lower frequency range can be tolerated. A direct comparison between both identifications after high-pass filtering—Figures 11(d) and 16(b)—shows only a slight improvement from the six-transducer set-up. However, the overall performance of this transducer array might be interesting when attempting to recover low-frequency information, for instance the remote beam motions.

7. CONCLUSIONS

In this paper, a method has been presented for the experimental identification of impact forces under complex rattling motions using remote measurements of the flexural waves. The conditioning of the identification problem was thoroughly discussed and guidelines are given concerning the number of transducers used in the identification procedure and their optimal location. The performance of the technique was asserted through extensive numerical simulations and experiments. From this work, the following conclusions may be drawn.

The classic Bernoulli–Euler beam theory is adequate for modelling wave propagation in the problem under concern. Damping effects can be safely neglected, for low-damped systems such as the one used in our tests.

The technique developed to separate wave reflections from the primary waves proved to be effective, even if waves other than those generated by the impacts are travelling along the system.

Important aspects to take in consideration are (1) the transducers should be located in such way that inversion is not plagued by ill-conditioning, and (2) the wave propagation constant $\mathscr{C}$ must be carefully adjusted.

Experiments show that transducers with excessive precision or phase matching are not required to achieve acceptable identification results.

In conclusion, the technique presented in this paper makes possible the identification of complex rattling forces from remote response measurements, even when measurements present noise contamination. Currently, this work is being extended to address the identification of impact forces in multi-supported systems.

ACKNOWLEDGMENTS

The experiments presented in this paper were performed with the valuable assistance of Paulo de Araújo, from the Applied Dynamics Laboratory, Instituto Tecnológico e Nuclear (ITN/ADL, Sacavém, Portugal). The authors also thank the reviewers for their interesting comments, which helped to improve the presentation.

REFERENCES

1. R. J. Rogers and R. Pick 1977 *Nuclear Engineering and Design* **44**, 247–253. Factors associated with support forces due to heat exchanger tube vibration contact.
2. T. Frick, T. Sobek and R. Reavis 1984 *Symposium on Flow-Induced Vibration*, *ASME Winter Annual Meeting*, *New Orleans*, *LA*. Overview on the development and implementation of methodologies to compute vibration and wear of steam generator tubes.
3. M. Rao, G. Gupta, F. Eisinger, H. Hibbitt and D. Steininger 1987 *International Conference on Flow-Induced Vibrations*, *Bowness-on-Windermere*, *U.K*. Computer modelling of vibration and wear of multispan tubes with clearances at supports.
4. F. Axisa, J. Antunes and B. Villard 1988 *ASME Journal of Pressure Vessel Technology* **110**, 7–14. Overview of numerical methods for predicting flow-induced vibrations.
5. N. Fisher, M. Olesen, R. Rogers and P. Ko 1988 *International Symposium on Flow-Induced Vibration and Noise*, *ASME Winter Annual Meeting*, *Chicago*, *IL*. Simulation of tube-to-support dynamic interaction in heat exchanger equipment.
6. N. Mahutov, T. Fesenko and S. Kaplunov 1989 *International Conference on Engineering Aero-Hydroelasticity*, *Prague*, *Czechoslovakia*. Dynamics of systems in a liquid flow and structure durability.
7. J. Antunes, F. Axisa, B. Beaufils and D. Guilbaud 1990 *Journal of Fluids and Structures* **4**, 287–304. Coulomb friction modelling in numerical simulations of vibration and wear work rate of multi-span heat-exchangers.
8. F. Axisa, J. Antunes and B. Villard 1990 *Journal of Fluids and Structures* **4**, 321–341. Random excitation of heat-exchanger tubes by cross-flow.
9. E. de Langre, B. Beaufils and J. Antunes 1991 *International Conference on Flow-Induced Vibrations*, *Brighton*, *U.K.*, *Proceedings of the Institute of Mechanical Engineers*, 253–262. The numerical prediction of vibrations in tube bundles induced cross-flow turbulence.
10. A. Fricker 1991 *International Conference on Flow-Induced Vibrations*, *Brighton*, *U.K.*, *Proceedings of the Institute of Mechanical Engineers*, 129–137. Vibro-impact behaviour of fluid-elastically unstable heat exchanger tubes with support clearances.
11. J. Antunes, E. de Langre, M. A. Vento and F. Axisa 1992 *Symposium on Flow-Induced Vibration and Noise*, *Anaheim*, *CA*, *ASME* **PVP-242**, 135–150. A theoretical model for the vibro-impact motion of tubes under fluidelastic instability.
12. E. de Langre, C. Hadj-Sadok and B. Beaufils 1992 *Symposium on Flow-Induced Vibration and Noise*, *Anaheim*, *CA*, *ASME* **PVP-242**, 107–131. Nonlinear vibrations induced by fluidelastic forces in tube bundles.
13. Th. Payen and E. de Langre 1996 *ASME Pressure Vessel and Piping Conference*, *Montreal*, *Canada*, *ASME* **PVP-328**, 337–346. A probabilistic approach for the computation of nonlinear vibrations of tubes under cross-flow.
14. R. G. Sauvé 1996 *ASME Pressure Vessel and Piping Conference*, *Montreal*, *Canada*, *ASME* **PVP-328**, 327–335. A computational time domain approach to fluidelastic instability for nonlinear tube dynamics.

15. X. Tan and R. J. Rogers 1996 *ASME Pressure Vessel and Piping Conference*, *Montreal*, *Canada*, *ASME* **PVP-328**, 347–358. Dynamic friction modelling in heat exchanger tube simulations.
16. M. Yetisir and N. Fisher 1996 *ASME Pressure Vessel and Piping Conference*, *Montreal*, *Canada*, *ASME* **PVP-328**, 359–368. Fretting-wear prediction in heat exchanger tubes: the effect of chemical cleaning and modelling ill-defined support conditions.
17. T. Zhou and R. J. Rogers 1996 *ASME Pressure Vessel and Piping Conference*, *Montreal*, *Canada*, *ASME* **PVP-328**, 257–270. Simulation of two-dimensional squeeze film and solid contact forces acting on a heat exchanger tube.
18. F. Axisa, A. Desseaux and R. G. Gibert 1984 *Symposium on Flow-Induced Vibration*, *ASME Winter Annual Meeting*, *New Orleans*, *LA*. Experimental study of the tube/support impact forces in multi-span PWR steam generator tubes.
19. S. S. Chen, J. Jendrzejczyk and M. Wamsganss 1984 *Symposium on Flow-Induced Vibration*, *ASME Winter Annual Meeting*, *New Orleans*, *LA*. Dynamics of tubes in fluid with tube-baffle interaction.
20. J. Cha, M. Wamsganss and J. Jendrzejczyk 1986 *ASME Pressure Vessel and Piping Conference*, *Chicago*, *IL*. Experimental study on impact/fretting wear in heat exchanger tubes.
21. K. Haslinger, M. Martin and D. Steininger 1987 *International Conference on Flow-Induced Vibrations*, *Bowness-on-Windermere*, *U.K.* Pressurised water reactor steam generator tube wear prediction utilising experimental techniques.
22. J. Antunes, F. Axisa and M. Vento 1992 *ASME Journal of Pressure Vessel Technology* **114**, 23–32. Experiments on tube/support interaction with feedback-controlled instability.
23. F. Axisa and P. Izquierdo 1992 *Symposium on Flow-Induced Vibration and Noise*, *Anaheim*, *CA*, *ASME* **PVP-242**, 281–300. Experiments on vibro-impact dynamics of loosely supported tubes under harmonic excitation.
24. M. A. Vento, J. Antunes and F. Axisa 1992 *Symposium on Flow-Induced Vibration and Noise*, *Anaheim*, *CA*, *ASME* **PVP-242**, 151–166. Tube/support interaction under simulated fluidelastic instability: two-dimensional experiments and computations of the nonlinear responses of a straight tube.
25. K. Boucher and C. Taylor 1996 *ASME Pressure Vessel and Piping Conference*, *Montreal*, *Canada*, *ASME* **PVP-328**, 285–296. Tube support effectiveness and wear damage assessment in the u-bend region of nuclear steam generators.
26. E. de Langre and G. Lebreton 1996 *ASME Pressure Vessel and Piping Conference*, *Montreal*, *Canada*, *ASME* **PVP-328**, 317–325. An experimental and numerical analysis of chaotic motion in vibration with impact.
27. N. Fisher, J. Tromp and B. Smith 1996 *ASME Pressure Vessel and Piping Conference*, *Montreal*, *Canada*, *ASME* **PVP-328**, 271–283. Measurement of dynamic interaction between a vibrating fuel element and its support.
28. N. Mureithi, T. Ito and T. Nakamura 1996 *ASME Pressure Vessel and Piping Conference*, *Montreal*, *Canada*, *ASME* **PVP-328**, 19–24. Identification of fluidelastic instability under conditions of turbulence and nonlinear tube supports.
29. G. S. Whiston 1984 *Journal of Sound and Vibration* **97**, 35–51. Remote impact analysis by use of propagated acceleration signals: I—theoretical methods.
30. R. W. Jordan and G. S. Whiston 1984 *Journal of Sound and Vibration* **97**, 53–63. Remote impact analysis by use of propagated acceleration signals: II—Comparison between theory and experiments.
31. J. Doyle 1989 *Wave Propagation in Structures*: *An FFT-Based Spectral Analysis Methodology*. New-York: Springer-Verlag.
32. S. Q. Lin and C. N. Bapat 1992 *Journal of Sound and Vibration* **157**, 485–513. Estimation of clearances and impact forces using vibroimpact response: sinusoidal excitation.
33. S. Q. Lin and C. N. Bapat 1993 *Journal of Sound and Vibration* **163**, 407–421. Estimation of clearances and impact forces using vibroimpact response: random excitation.
34. S. Q. Lin and C. N. Bapat 1993 *Journal of Sound and Vibration* **163**, 423–428. Extension of clearance and impact force estimation approaches to a beam–stop system.
35. H. R. Busby and D. M. Trujillo 1987 *Computers and Structures* **25**, 109–117. Solution of an inverse dynamics problem using an eigenvalue reduction technique.
36. E. Wu and J. C. Yeh 1994 *A.I.A.A. Journal* **32**, 2433–2439. Identification of impact forces at multiple locations on laminated plates.
37. J. T. Kim and R. H. Lyon 1992 *Mechanical Systems and Signal Processing* **6**, 1–15. Cepstral analysis as a tool for robust processing, deverberation and detection of transients.

38. M. DE ARAÚJO, J. ANTUNES and P. PITEAU 1998 *Journal of Sound and Vibration* **215**, 1015–1041. Remote identification of impact forces on loosely supported tubes: Part 1—basic theory and experiments.
39. W. H. PRESS, A. A. TEUKOLSKY, W. T. VETTERLING and B. P. FLANNERY 1992 *Numerical Recipes*: *The Art of Scientific Computing*. Cambridge: Cambridge University Press.
40. C. W. GROETCH 1993 *Inverse Problems in the Mathematical Sciences*. Wiesbaden: F. Vieweg & Sohn.
41. P. C. HANSEN 1994 *Numerical Algorithms* **6**, 1–35. Regularisation tools.
42. W. JEFFREY and R. ROSNER 1986 *The Astrophyical Journal* **310**, 463–472. On strategies for inverting remote sensing data.
43. V. DIMRI 1992 *Deconvolution and Inverse Theory*: *Application to Geophysical Problems*. Amsterdam: Elsevier.
44. R. L. PARKER 1994 *Geophysical Inverse Theory*. Princeton, NJ: Princeton University Press.
45. P. M. MORSE and K. U. INGARD 1968 *Theoretical Acoustics*. Princeton, NJ: Princeton University Press.
46. K. F. GRAFF 1975 *Wave Motion in Elastic Solids*. London: Oxford University Press.
47. M. C. JUNGER and D. FEIT 1986 *Sound*, *Structures and Their Interaction*. Cambridge, MA: M.I.T. Press.
48. V. I. BABITSKY and V. L. KRUPENIN 1985 *Oscillations in Strongly Non-linear Systems*. Moscow: Nauka.
49. V. L. KRUPENIN and A. M. VEPRIK 1996 2*nd European Nonlinear Oscillation Conference*, *Prague*, *Czechoslovakia*. Vibroconductors equipped with impact elements and distributed vibroimpact systems.
50. C. K. CHUI 1992 *An Introduction to Wavelets*. San Diego: Academic Press.
51. J. LINJAMA and T. LAHTI 1992 *Journal of Sound and Vibration* **153**, 21–36. Estimation of bending wave intensity in beams using the frequency response technique.
52. F. J. FAHY 1995 *Sound Intensity*. London: E & FN Spon.
53. C. HALKYARD and B. MACE 1995 *Journal of Sound and Vibration* **185**, 279–298. Structural intensity in beams—waves, transducer systems and the conditioning problem.
54. V. GIBIAT and F. LALOË 1990 *Journal of the Acoustical Society of America* **88**, 2533–2545. Acoustical impedance measurements by the two-microphone-three-calibration (TMTC) method.

APPENDIX: NOMENCLATURE

A	area of the beam cross-section
C_n	wave amplitude parameters
c_n	phase speed of the waves
$\mathscr{C}$	frequency parameter of k_n
E	Young's modulus of the beam
$F_y(t)$	external force
F_n	spectral coefficients of the external force
$\mathscr{F}$, $\mathscr{F}^{-1}$	direct and inverse Fourier transforms
$G(x, \omega_n)$	wave-to-wave transfer function
$\tilde{G}(x, \omega_n)$	force-to-wave transfer function
I	moment of inertia of the cross-section
$k_n = F(\omega_n)$	dispersion relation of the waves
N	axial tension on the beam
t	time
x	location along the beam
$y(x, t)$	flexural beam response
y_b	backward going wave
y_f	forward going wave
Y_n	spectral coefficients of the wave
ρ	mass density of the beam
η	viscosity coefficient
ω_n	circular frequency